This article has been accepted for publication and undergone full peer review but has not been through the copyediting, typesetting, pagination and proofreading process, which may lead to differences between this version and the Version of Record. Please cite this article as doi: 10.1002/advs.202000...

This article is protected by copyright. All rights reserved.

Acce

This article is protected by copyright. All rights reserved.

.85 41.176 214.66 43.664 213.559.86 c.506 2human.85 41.176 214.66 43.66105.71 59.86 c.506 2-.85 41.176 214.66 43.66101.78 59.86 c.506 2ree

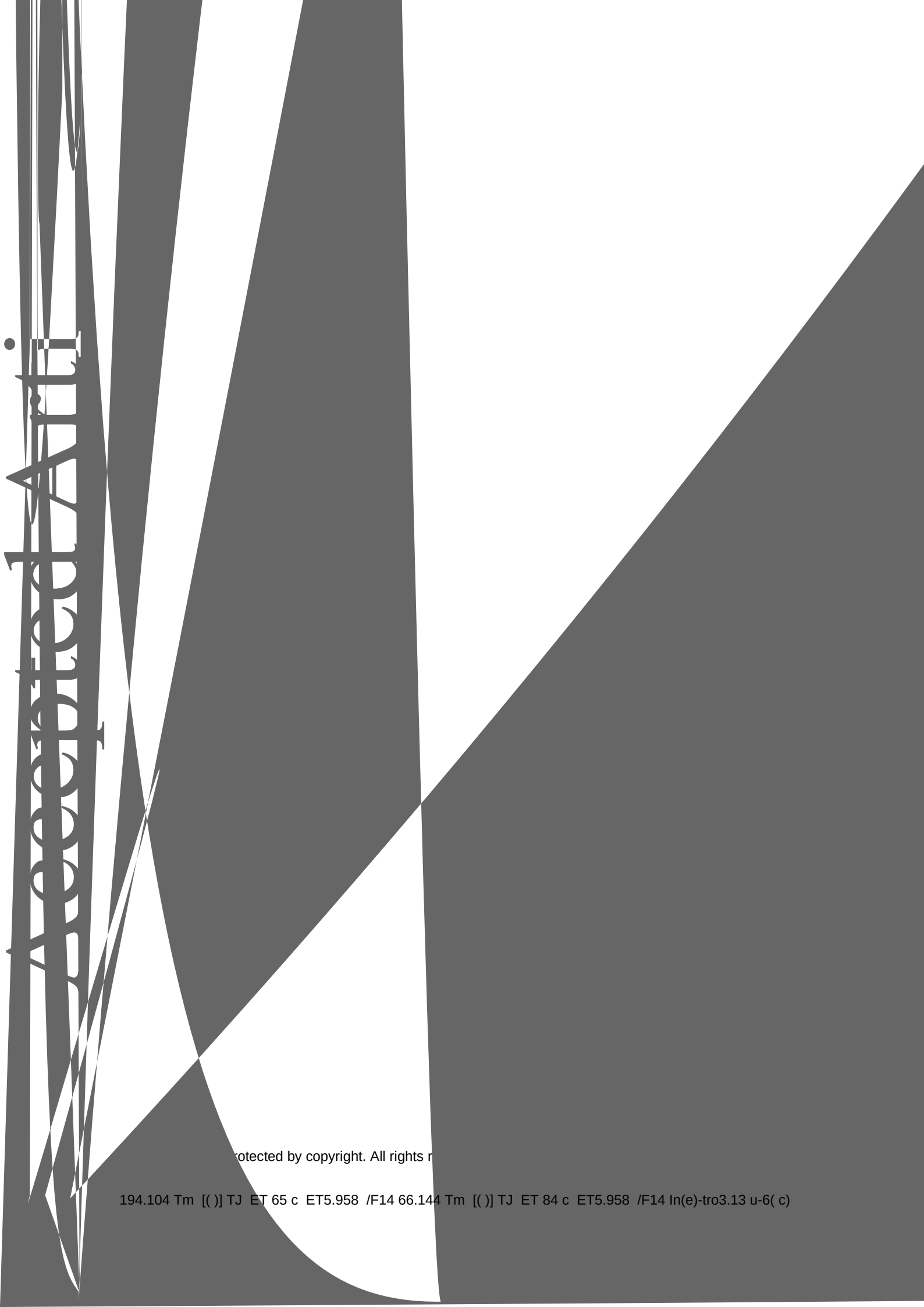

otected by copyright. All rights r

194.104 Tm [( )] TJ ET 65 c ET5.958 /F14 66.144 Tm [( )] TJ ET 84 c ET5.958 /F14 In(e)-tro3.13 u-6(c)

Accepted Article

systemic responses to SARS-CoV-2 infection may be significantly different from that of human individuals. Moreover, expensive costs, time-consuming processes and animal ethics should be carefully considered. As such, it is highly desirable to develop alternative preclinical models to better reflect the pathophysiology of human organs to accelerate SARS-CoV-2 research and the development of COVID-19 candidate therapeutics.

Significant advances in bioengineered organs-on-chips technology have made it possible to reconstruct 3D human organotypic models *in vitro* by recapitulating the key functions of living organisms in microfluidic culture devices, such as intestine, heart, liver and lung et al.[17-21] They can resemble the organ physiology in a human-relevant manner, holding great potentials in disease studies, drug testing and virology.[17, 22-25] Inberg ¶ group successfully proposed the engineered lung-on-chips in a multilayered microfluidic device that enables to reconstitute the air-liquid interfaces[17] and applied them to study respiratory diseases, such as pulmonary edema[26], asthma and toxicity assessment.[27] Other types of lung chip models were developed to reproduce alveolar-capillary interfaces with flexible configurations to assess the environmental pollutants induced toxicity.[24, 28] More recently, lung chip was also attempted to study the study the host-virus interactions by influenza virus and pseudotyped SARS-CoV-2, and screen approved drugs as potential therapeutics.[23, 29] Junaid et al reported the modeling of Ebola hemorrhagic syndrome in a microvessel-on-a-chip system to test the effect of candidate drugs.[30]

According to clinical findings, lung is the primary target organ in the progress of COVID-19. *In vivo*, alveoli is the core functional unit of lung, in which the alveolar-capillary barrier plays a vital role in maintaining gas exchange and preventing the invasion of external hazardous substances or virus infection (**Figure 1**A). This functional barrieris mainly composed of human alveolar epithelial and vascular endothelial cells that interact across a 3D extracellular matrix (ECM). More clinical evidences indicate that SARS-CoV-2 infection can damage alveolar function in severe patients. In order to create the human lung infection model by SARS-CoV-2 *in vitro*, we initially designed and constructed a biomimetic human

This article is protected by copyright. All rights reserved.

AC

This article is protected by copyright. All rights reserved.

Acce

This article is protected by copyright. All rights reserved.

Accepted Article

suggested that SARS-CoV-2 can primarily infect and replicate in the alveolar epithelial cells, but not in endothelial cells.

2.3. Transcriptional analysis of host cells responses to SARS-CoV-2 infection

In order to fully understand the transcriptional responses to SARS-CoV-2 infection, we performed RNA-seq analysis of HPAEpiC and HULEC-5a cells following viral infection in the alveolus chip. Briefly, 3 days after infection, HPAEpiC cells and HULEC-5a cells were collected separately and analyzed by RNA-sequencing. Firstly, the ratio of virus-aligned reads over total reads in each sample was calculated to estimate the viral replication levels in these two cell types. The results showed that the ratio of viral reads in HPAEpiC cells is much higher than HULEC-5a cells (**Figure 4**A and B), which are consistent with the western blot (**Figure 2**B) and immunostaining analysis (Figure 3B). It revealed that human alveolar epithelial cells were more permissive to SARS-CoV-2 infection than microvascular endothelial cells, similar to the histopathological findings from autopsy reports.[37]

Volcano plots showed that SARS-CoV-2 infection induced global transcriptome modulations in both HPAEpiC cells and HPAEpiC cells (Fig**ure 4**C). To identify the differentially expressed genes (DEGs) in the two cell types, the cut-off values for the fold change and P value were set to 2.0 and 0.05, respectively. Among the DEGs, 972 genes (324 down-regulated genes and 648 up-regulated genes) were significantly modulated in HPAEpiC cells, while 735 genes (495 down-regulated genes and 240 up-regulated genes) were significantly modulated in HULEC-5a cells. By combining the two data sets, we found the two cell types only shared 52 overlapping up-regulated DEGs (6.2% of total up-regulated DEGs) and only 43 overlapping down-regulated DEGs (5.5% of total down-regulated DEGs) (**Figure 4**D). These results suggested that the alveolar epithelial and pulmonary microvascular endothelial cells showed distinct transcriptional responses to SARS-CoV-2 infection.

This article is protected by copyright. All rights reserved.

Accepted Article

To better understand the host responses to SARS-CoV-2 infection, Gene Ontology (GO) enrichment analysis was performed to identify biological processes enriched among significantly regulated genes. It appeared the distinctive GO terms were enriched between HPAEpiC cells and HULEC-5a cells following viral infection. Notably, among the top 20 enriched terms, the biological processes associated with epithelial cell apoptosis, cell division and mitotic cell cycle were particularly enriched in HPAEpiC cells (**Figure 4**E). While, in HULEC-5a cells, the biological processes involved in cytokinesis, transcriptional factor activity, chemotaxis were significantly modulated (**Figure 4**F).

In general, viral infection can trigger antiviral or immune responses in host cells. In order to identify the specific host defense responses to SARS-CoV-2 infection, we then searched the genes related with immune responses from the up-regulated DEGs according to GO annotation, and performed GO enrichment analysis. The results demonstrated distinct immune responses induced by this virus in the two cell types. It is noted, SARS-CoV-2 infection induced a broad innate immune response and antiviral responses, including defense response to virus, type I interferon (IFN-I) signaling pathway and cytokine-mediated signaling pathway in HPAEpiC cells, (**Figure 5**A). While, the terms related to the positive regulation of JAK-STAT cascade and adaptive immune response were particularly enriched in HULEC-5a cells, (**Figure 5**B). Moreover, among the up-regulated genes associated with immune responses, we identified some cytokines, including IL-16, IL-11 and CXCL11 in HPAEpiC cells (**Figure 5**C), and CCL15-CCL14, CCL15 and CCL23 in HULEC-5a (**Figure 5**D).

Collectively, these findings revealed SARS-CoV-2 infection exhibited distinct effects on alveolar epithelial cells and microvascular endothelial cells, including the susceptibility to virus, immune responses and activated signaling pathways. These data reflect the diverse responses of human alveolar epithelial and endothelial cells to viral infection, which may explain the possible complex cross-talk of host cells involved in the pathogenesis of COVID-19.

This article is protected by copyright. All rights reserved.

Accepted Article

2.4. Immune responses in human alveolus chip following SARS-CoV-2 infection

The accumulation and extensive infiltration of immune cells in the lungs may contribute significantly to the pathogenesis in patients infected with respiratory viruses.[38] We next explored the roles of human circulating immune cells in the alveolar pathological process after SARS-CoV-2 infection. In this study, PBMCs were isolated from healthy human blood

This article is protected by copyright. All rights reserved.

Accepted Article

infiltration in lungs as observed clinically.[9, 39] In addition, we also applied the non-specific stimulants (e.g., IL-2 and IL-6) on the alveolar chip to identify the response of human immune cells to these stimulators. The immune cells were introduced into the vascular channel of the chip after IL-2 or IL-6 (30 ng/mL) treatment for 2 days. More immune cells were observed to be attached to the pulmonary microvascular endothelium induced by IL-6, which is similar to the recruitment of immune cells in the vascular side induced by SARS-CoV-2 infection in our chip model. These results suggest that inflammatory factors (e.g., IL-6) may play a crucial role in the activated immune response of host cells to viral infection (supplementary Figure S5).

To further explore the inflammatory responses induced by SARS-CoV-2 in this model system, we evaluated the release of several pro-inflammatory cytokines from culture media in the vascular channel. At 2 days post-infection, the levels of IL-6 and IL-8 were significantly increased in the absence of PBMCs (Figure 6G and H). Moreover, all four cytokines (IL-IL-6, IL-8 and TNF- D) were markedly increased following SARS-CoV-2 infection with the incorporation of PBMCs (Figure 6F-I). Especially, viral infection caused a 10-fold increase of IL- D Q G-6 level in the culture medium from the lower endothelium layer as compared to the group without infection (Figure 6F and G). Similarly, the increased secretion of these inflammatory cytokines from upper epithelium layer were also detected (supplementary Figure S4). Clearly, SARS-CoV-2 infection in this alveolar chip could induce the recruitment of PBMCs, and aggravated inflammatory response in lung tissue as observed in clinics, demonstrating the feasibility of this microengineered lung model system to reflect the human-relevant pathophysiology of COVID-19.

2.5. Assessment of potential anti-viral therapeutics

To assess the potential therapeutics against SARS-CoV-2, we treated the virus infected human alveolus chip with remdesivir. Remdesivir is recognized as a promising antiviral

This article is protected by copyright. All rights reserved.

Accepted Article

This article is protected by copyright. All rights reserved.

Accepted Article

As we know, alveolar epithelial type II cells have been proved to be the primary target of SARS-CoV-2 infection by histopathological studies.[43] In this study, we found that human alveolar epithelial cells are more susceptible to SARS-CoV-2 infection than endothelial cells identified on the chip. Moreover, transcriptomic analysis demonstrated the distinctive responses of alveolar epithelial and endothelial cells to SARS-CoV-2 infection, in which epithelium exhibited much higher viral load than that of endothelium. This may partially explain why SARS-CoV-2 cannot be easily detected in blood samples of COVID-19 patients.[37] In addition, compared with pulmonary microvascular endothelial cells, alveolar epithelial cells displays a broader innate immune response after viral infection, such as IFN-I signaling pathway. A recent study reported the IFN-I responsive gene sets were up-regulated in lung tissues from severe COVID-19 cases, which may be associated with exacerbated lung inflammation.[44] Our results are similar to these clinical findings, indicating the advantage of this disease model to reflect the human relevant immune responses of lung. Meanwhile, we detected the activation of JAK-STAT signaling pathway in the infected pulmonary microvascular endothelial cells as compared to non-infected cells. It has been recognized that cytokines can activate JAK-STAT pathway and regulate different cellular and immune processes.[45, 46] Clinical studies reported Ruxolitinib, a JAK inhibitor can effectively relieve the symptoms of patients with severe COVID-19.[47, 48] In combination with these findings, it might suggest the feasibility to develop new therapeutics against SARS-CoV-2 by targeting JAK-STAT signaling pathway in microvascular endothelium.

Clinically, severe COVID-19 patients often show inflammatory cytokine storms, which are associated with excessive immune responses, and may aggravate respiratory failure and cause multi-organ damage. Circulating cytokines, including IL- ,-6, IL-8 and TNF- . were significantly elevated in patients with severe COVID-19.[49, 50] As such, we compared the secretion of these cytokines in this alveolus chip under different treatment conditions. Our results showed that SARS-CoV-2 infection triggered the increased secretions of cytokines IL-6, and IL-8 on the alveolus chip. In particular, the addition of circulating immune cells caused the increased level of all these cytokines secretion, accompanied by recruitment of

This article is protected by copyright. All rights reserved.

Accepte

This article is protected by copyright. All rights reserved.

Accepted Artic

This article is protected by copyright. All rights reserved.

Accepted Article

lumen and the microvascular layer, respectively. The length of the overlapping channels is 15 mm. The two channels are separated by a thin (~25 μm thick) PDMS membrane (5 μm pore diameter and 70 μm between pores) to construct the tissue-tissue interface (supplementary figure S1). The porous PDMS membranes were fabricated based on the glass templates and spin-coating method modified from the previous protocol. The membrane was sandwiched between the aligned upper and bottom channels of the device by oxygen plasma bonding for 30 s. Finally, the chip devices were sterilized in an autoclave and the porous member of the device was coated with rat tail collagen type I (200 μg/mL, Corning) on both sides at 37 °C for 48 h before cell seeding.

Cell culture and lab consumables: African green monkey kidney epithelial Vero E6 cells (ATCC No. CRL-1586) were cultured in Dulbecco's Modified Eagle's Medium (DMEM, Gibco) supplemented with 10% Fetal Bovine Serum (FBS, Gibco). Immortalized human alveolar epithelial cells (HPAEpiC) were generated from Type II pneumocytes of human lung tissue (purchased form Sciencell Shanghai Corporation) and were maintained in RPMI 1640 medium (Gibco) supplemented with 10% FBS. Human lung microvasculature cell line HULEC-5a was purchased from Procell Corporation and were maintained in HULEC-5a growth medium (Procell, CM-0565). Human peripheral blood mononuclear cells were isolated from fresh human blood using Ficoll (Stem cell technologies) density centrifugation. Isolated PBMCs were re-suspended in RPMI 1640 medium containing 10% FBS and 50 IU/mL IL-2 and used for adhesion assays on chip. All cells were cultured at 37 °C in a humidified atmosphere of 5% CO_2.

To create the human alveolus chip, HULEC-5a cells (~ 1×10^5 cells) were initially seeded on the bottom side of the collagen-coated porous PDMS membrane and then attached to the membrane surface under static conditions for two hours. Subsequently, cells were washed with fresh medium to exclude/remove unattached ones. Then, HPAEpiC cells (~ 5×10^5 cells) were seeded into the upper channel under static culture. After cell attachment, constant media

This article is protected by copyright. All rights reserved.

AC

This article is protected by copyright. All rights reserved.

This article is protected by copyright. All rights reserved.

Accepted Article

immunofluorescence staining by the same procedure as described above. All images were acquired using a confocal fluorescent microscope system (Carl zeiss LSM880). Image processing was done using ImageJ (NIH).

Analysis of inflammatory cytokines: To analyze the released cytokines, the media in the vessel channel were collected from each chip. The concentrations of IL-6, IL-8, IL- D Q G TNF- Dwere measured using the corresponding human ELISA kits (Biolegend, USA) D F F R U G L Q J W R W K H P D Q X I D F W X U H U ¶ V L Q V W U X F W L R Q V

Real-time quantitative PCR (qRT-PCR): Virus titers were determined by viral RNA detection using qRT-PCR. The culture supernatant for each condition was harvested for RNA extraction using the HP Viral RNA Kit (Roche, Cat no. 11858882001) according to the P D Q X I D F W X U H U ¶ V - PCR was performed using One-Step RT-PCR RNA direct real-time PCR master mix (TOYOBO, QRT-101A) in a PCR System (Applied Biosystem, 9 L L \$ Œ 7 K H S U L P HU V HTU Ge w e e as follows: N-) -¶GG GAA CTT CTC CTG CTA GAA T- ¶ -5 -¶AG ACA TTT TGC TCT CAA GCT G- ¶ -probe: ¶TTG CTG CTG CTT GAC AGA TT- ¶ 3 & 5 D P S O L I L F D W L R Q Z D V S H U I R U P H following conditions: 50 (for 10 min, and 95 (1min, followed by 45 cycles consisting of 95 (for 15 s, 60 (for 45 s.

Transmission electron microscopy: HPAEpiC cells were collected and fixed in 4% PFA (Electron Microscopy Sciences) and 2.5% glutaraldehyde (Electron Microscopy Sciences) at 4 (overnight. After washed with PBS for three times and fixed in 1% OsO4 buffer for 2 h, the samples were dehydrated with graded ethanol solutions, and embedded in Epon 812 resin

This article is protected by copyright. All rights reserved.

Accepted Article

(SPI). Ultrathin sections (70 nm) were stained with 2% uranyl acetate for 30 minutes and then lead citrate for 10 mins. Images were acquired with a JEM-1400 PLUS electron microscope.

Remdesivir treatment: Stock solution of remdesivir (GS-5734) was prepared in DMSO. For the HPAEpiC cell culture on the plate, after SARS-CoV-2 infection for 1 h, the cells were treated with or without 1 μM remdesivir for 3 days and the supernatants were collected at distinct time points (24 h, 48 h and 72 h) for viral load analysis by qRT-PCR. For alveolus chip, cells were treated with or without 1 μM remdesivir for 2 days after SARS-CoV-2 infection in the presence of PBMCs. After 48 h, the cells were fixed for immunofluorescence analysis.

RNA extraction, library preparation and sequencing: HPAEpiC cells and HULEC-5a cells were collected separately from the chips, and total RNAs were extracted from samples using TRIzol (Invitrogen) following the methods by Chomczynski et al.[55] DNA digestion was carried out after RNA extraction by DNaseI. RNA quality was determined by examining A260/A280 with NanodropTM OneCspectrophotometer (Thermo Fisher Scientific Inc). RNA Integrity was confirmed by 1.5% agarose gel electrophoresis. Qualified RNAs were finally quantified by Qubit 3.0 with QubitTM RNA Broad Range Assay kit (Life Technologies). 500 ng total RNAs were used for stranded RNA sequencing library preparation using KC-DigitalTM Stranded mRNA Library Prep Kit for Illumina® (Catalog NO. DR08502, :XKDQ 6HT+HDOWK &R /WG &KLQD IROORZLQJ WKH PDQXID eliminates duplication bias in PCR and sequencing steps, using unique molecular identifier (UMI) of 8 random bases to label the pre-amplified cDNA molecules. The library products corresponding to 200-500 bps were enriched, quantified and finally sequenced on Hiseq X 10 sequencer (Illumina).

This article is protected by copyright. All rights reserved.

Acce

This article is protected by copyright. All rights reserved.

Accepted Article

bars represent mean ± standard deviation (SD). Significance is indicated by asterisks: *, $p < 0.05$; **, $p < 0.01$; ***, $p < 0.001$.

Data availability: All relevant data are available in the manuscript or supporting information. All of the RNA-seq raw data have been deposited on SRA under the accession number PRJNA647532.

Supporting Information

Supporting Information is available from the Wiley Online Library or from the author.

Acknowledgments

We thank Prof. Yonggang Yao (Kunming Institute of Zoology, CAS) for his strong support on this work. We thank Prof. Shiyong Liu (University of Science and Technology of China) for providing remdesivir compound. We thank Ms. Yingqi Guo (Kunming Institute of Zoology, CAS) for help with the preparation of samples for electron microscopy analysis.

This research was supported by the Strategic Priority Research Program of the Chinese Academy of Sciences è Grant (Nos. XDA16020900 è XDB29050301, XDB32030200), National Key R&D Program of China (No. 2017YFB0405404), National Science and Technology Major Project (No. 2018ZX09201017-001-001), The National key Research and Development Program of China (2020YFC0842000), National Nature Science Foundation of China (Nos. 31671038, 31971373 è 81703470, 81803492), China Postdoctoral Science Foundation (No. 2019M660065), Innovation Program of Science and Research from the DICP, CAS (DICP I201934).

This article is protected by copyright. All rights reserved.

Accepted Article

&RQÀLFW RI ,QWHUHVW

7KH DXWKRUV GHFODUH QR FRQÀLFW RI LQWHUHVW

This article is protected by copyright. All rights reserved.

Accept

This article is protected by copyright. All rights reserved.

Accepted Article

Figure 2. Examination of SARS-CoV-2 infection in HPAEpiC cells. (A) Analysis of ACE2 and TMPRSS2 proteins expression levels in

This article is protected by copyright. All rights reserved.

Accepted Article

body. (D) TEM micrographs of SRAS-CoV-2-infected HPAEpiC cells. (i) The overall image of the infected cell. (ii) Clusters of viruses within cell body. (iii) Enlarged image of virus particles. Three independent experiments were performed (n=3).

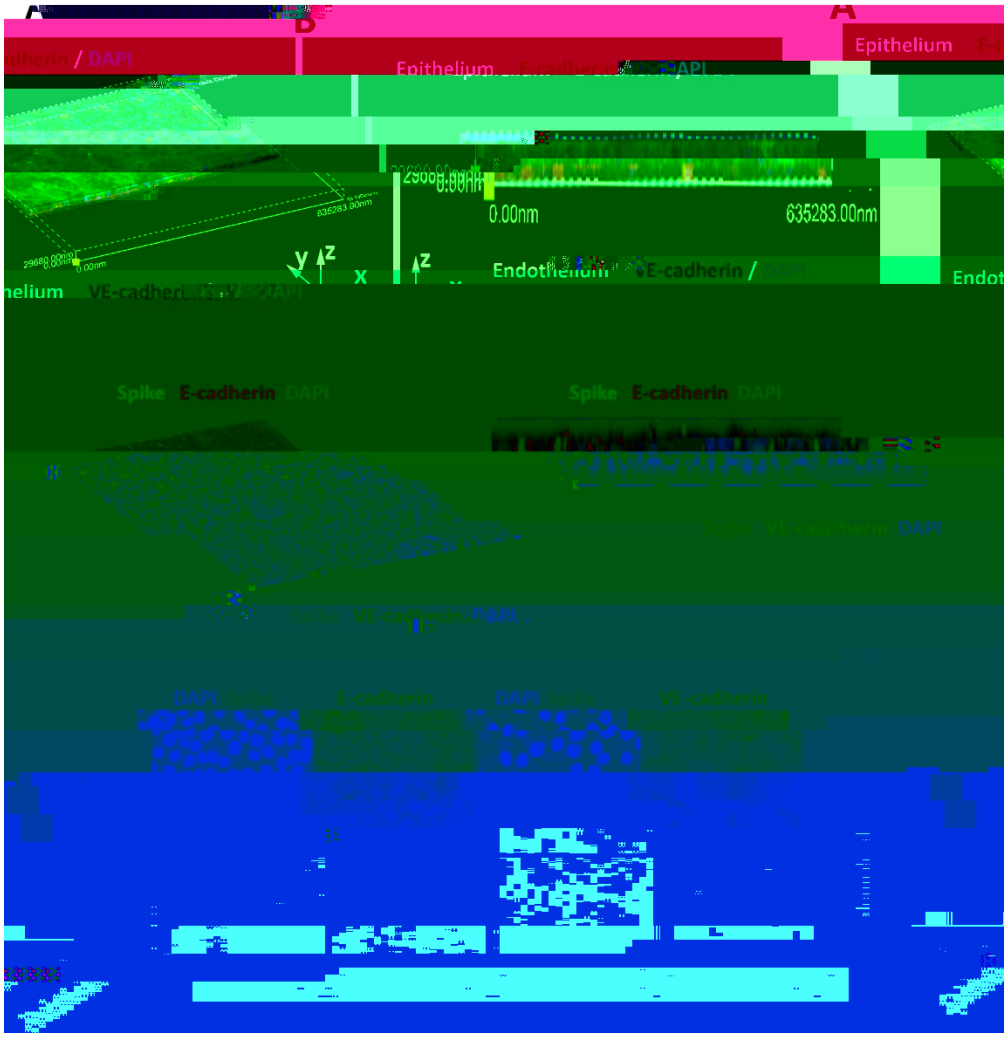

Figure 3. Characterization of infection and replication of SARS-CoV-2 in human alveolus chip. (A) 3D reconstructed confocal image of alveolar epithelium (E-cadherin) and pulmonary microvascular endothelium (VE-cadherin) in the alveolus chip. (B) Side view of alveolar epithelium (E-cadherin) and pulmonary microvascular endothelium (VE-cadherin). (C) 3D reconstructed confocal image of human alveolar-capillary-barrier at 3 days post-infection. (D) Side view of the formed alveolar barrier after viral infection. SARS-CoV-2 infection was predominantly identified in epithelium layer by viral Spike

This article is protected by copyright. All rights reserved.

Accepted Article

protein expression. (E) Confocal immunofluorescent micrographs showed the effects of SARS-CoV-2 infection (Spike protein) on the human epithelium (E-cadherin) and endothelium (VE-cadherin) of chip at 3 days post-infection. (F) Cell confluency of epithelium and endothelium on chip was examined with or without SARS-CoV-2 infection. Data were presented as mean ± SD. Three chips were quantified for each group.

This article is protected by copyright. All rights reserved.

Accepted Article

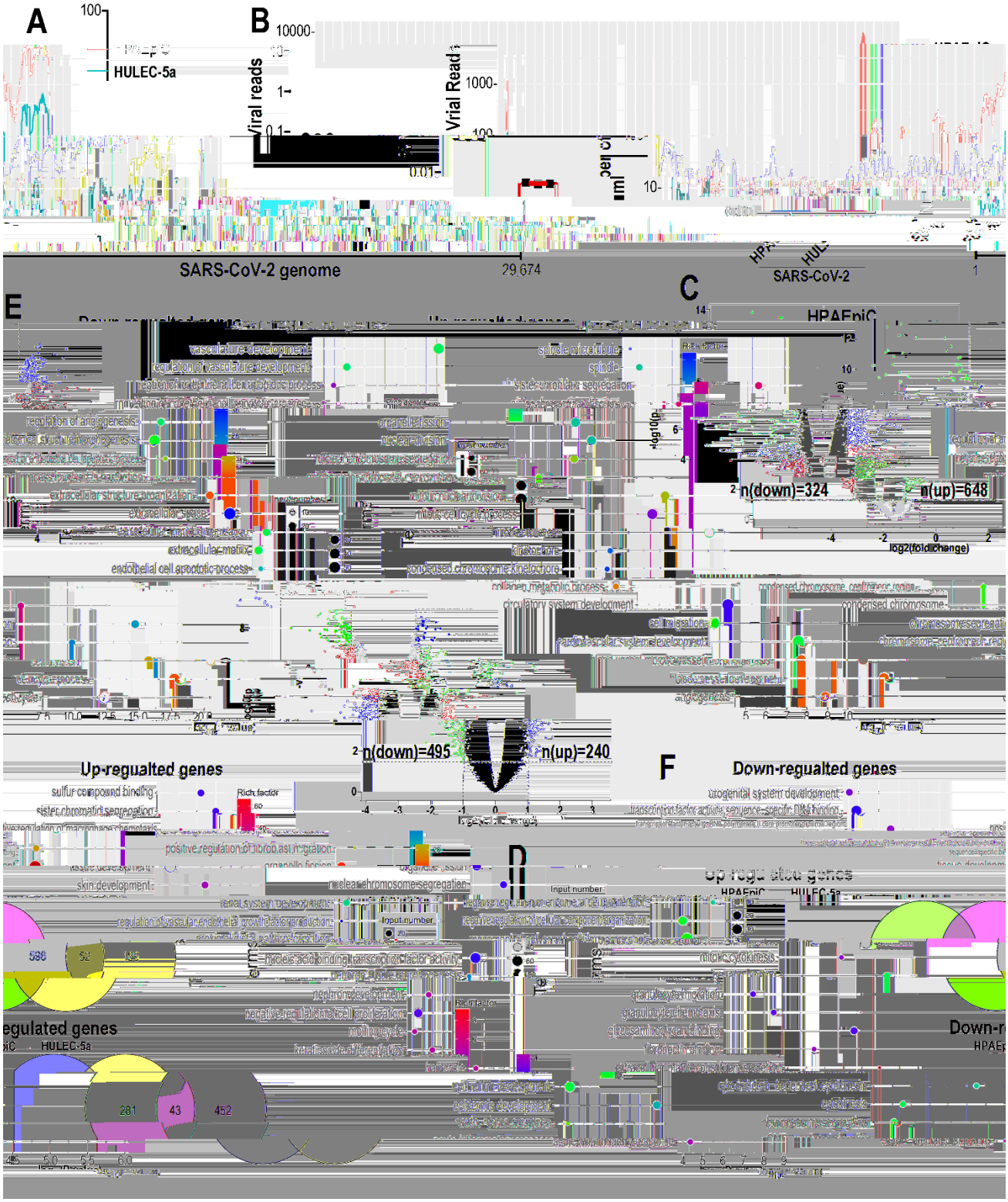

Figure 4. Transcriptional analysis of HPAEpiC cells and HULEC-5a cells to SARS-CoV-2 infection in human alveolus chip. (A) Viral replication levels in HPAEpiC and HULEC-5a

This article is protected by copyright. All rights reserved.

Acce

This article is protected by copyright. All rights reserved.

Accepted Article

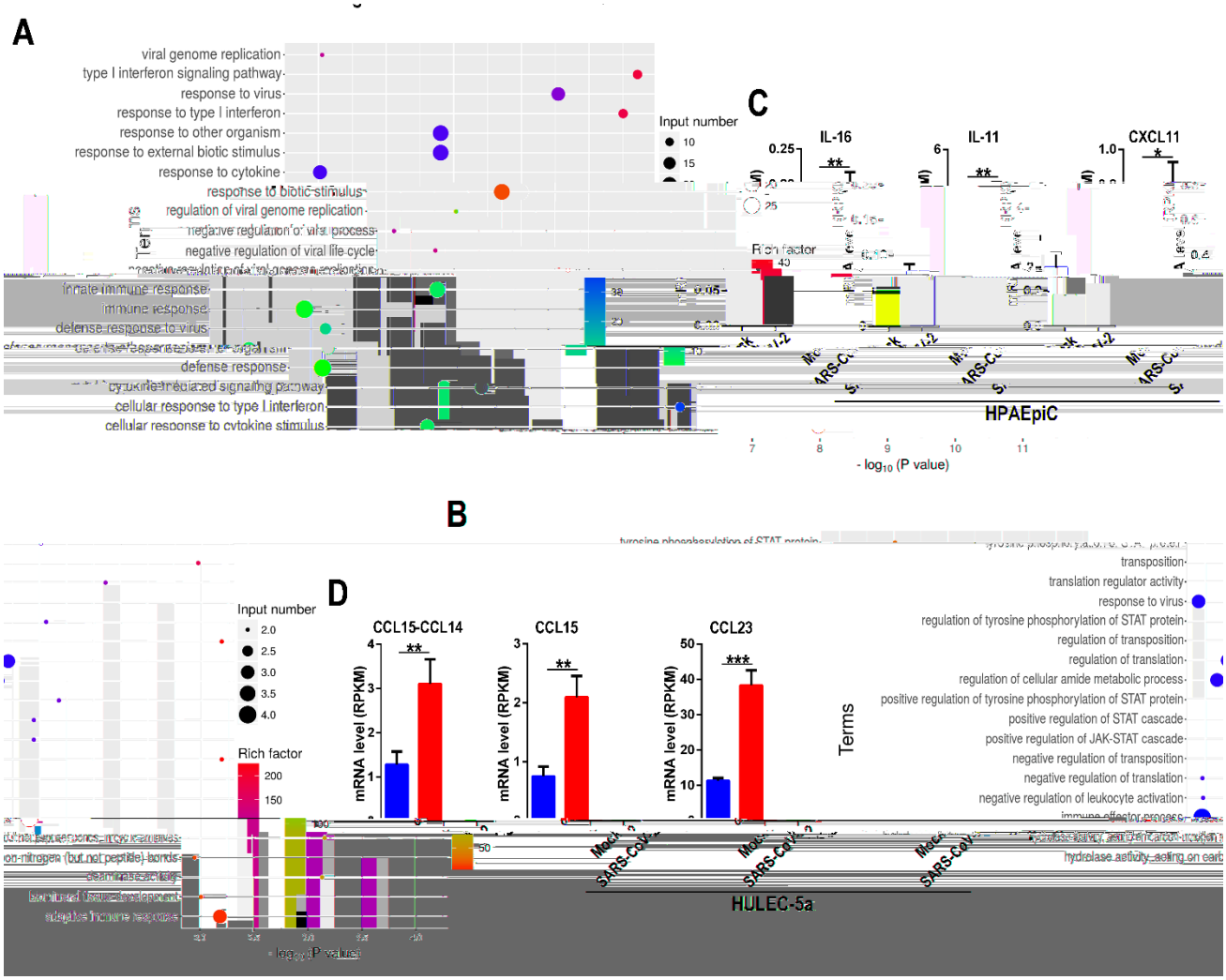

Figure 5. RNA-seq analysis showed distinctive immune responses to SARS-CoV-2 infection in co-cultured HPAEpiC cells and HULEC-5a cells on chip. (A) GO enrichment analysis of upregulated DEGs related with immune response in HPAEpiC cells after viral infection. (F) GO enrichment analysis upregulated DEGs related with immune response in HULEC-5a cells after viral infection. (C) Upregulated cytokines genes in HPAEpiC cells infected with virus by RNA-seq analysis. (D) Upregulated cytokines genes in HULEC-5a cells infected with virus by RNA-seq analysis. ' D W D Z H U H D Q D O \ ] H G (F \ 6 W X G H Q W ' W H V W ($ 1 2 9 $ p<0.05).

This article is protected by copyright. All rights reserved.

Accepted Article

This article is protected by copyright. All rights reserved.

Acce

This article is protected by copyright. All rights reserved.

Accepted Article

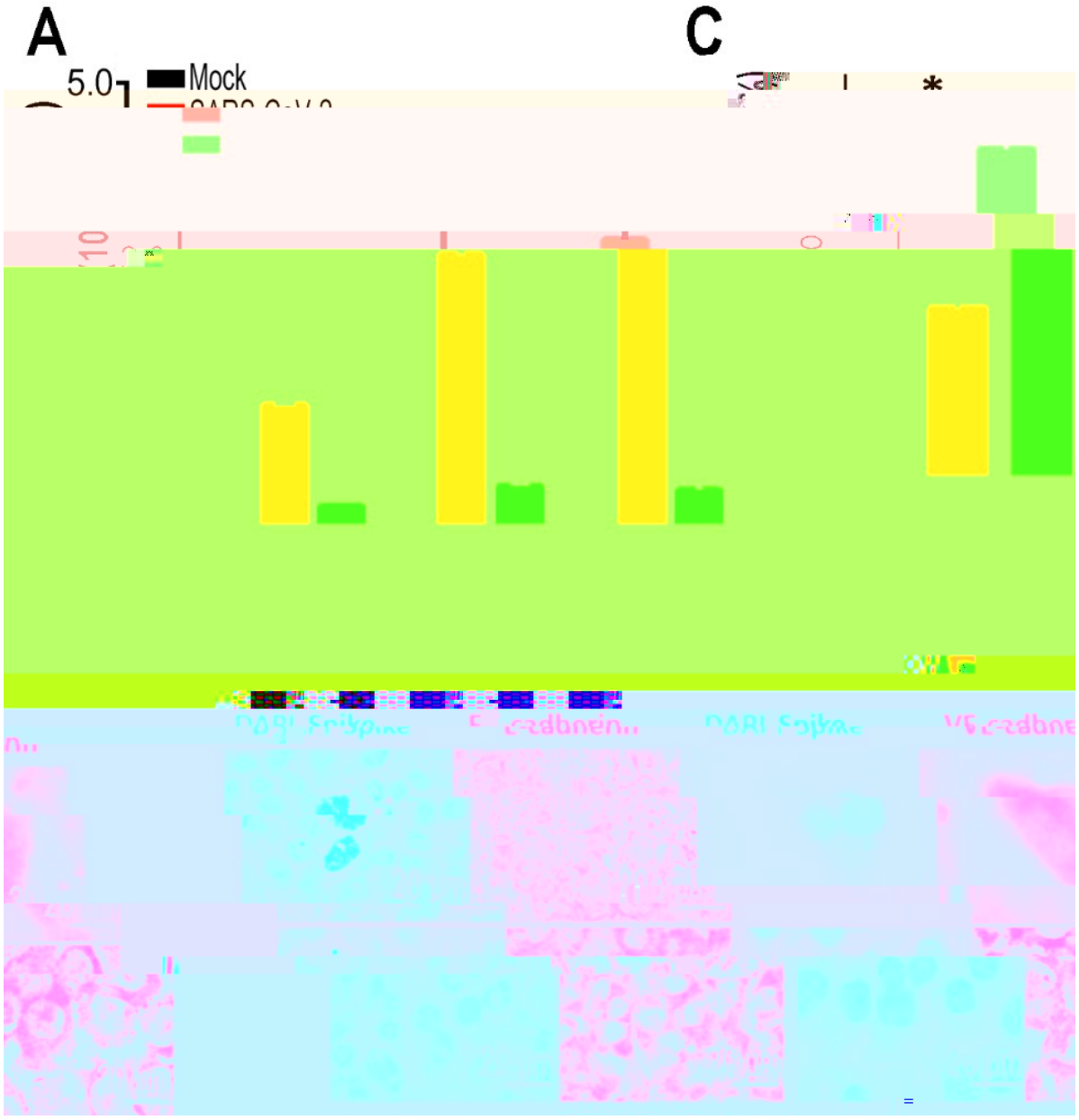

Figure 7. Evaluation of potential antiviral efficacy of remdesivir on the chip system. (A) Culture supernatants were harvested at indicated time points following SARS-CoV-2 infection to examine the viral load using qRT-PCR for different groups. The average of two independent experiments is shown. Data were presented as mean ± SD. (B) Confocal immunofluorescent micrographs of epithelium (E-cadherin) and endothelium (VE-cadherin) of alveolus chip treated without or with 0 remdesivir at 2 days post-infection. (C) Quantification for epithelial cell confluency of alveolus chip treated without or with 0

This article is protected by copyright. All rights reserved.

Accepted Article

remdesivir at 2 days post-infection. Three chips were quantified for each group. Data were

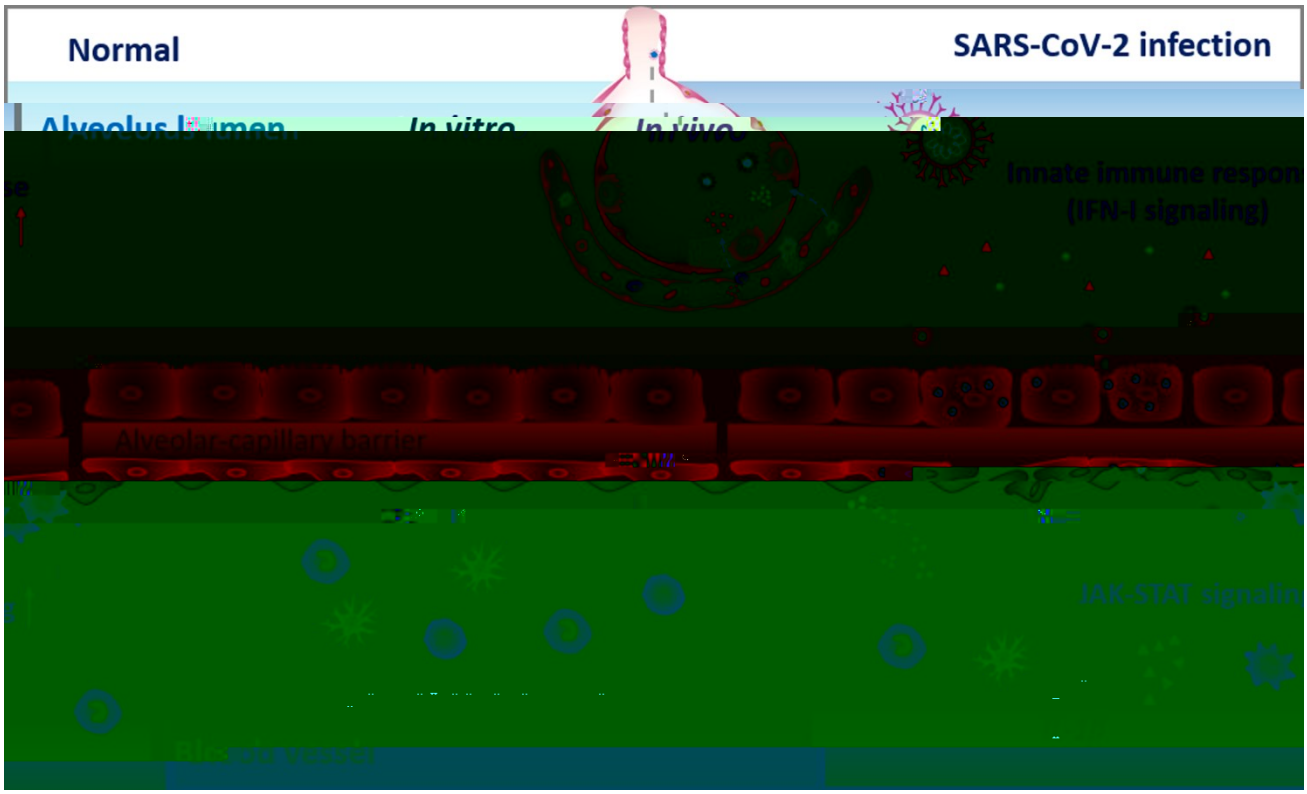

Figure 8. Schematic summary of SARS-CoV-2-induced lung injury and inflammatory responses associated with COVID 19 on the human organ chip model system. Following SARS-CoV-2 exposure, virus particles invade the alveolar epithelium and endothelium, and replicate violently in human epithelial cells. The viral infection can activate the host antiviral defense or immune response, including the activation of innate immune responses (e.g. IFN-I signaling pathway) in epithelial cells and JAK-STAT signaling pathway in endothelial cells. The cytokines or chemokines released from infected cells can recruit circulating immune cells (such as $CD14^+$ monocytes) to infected sites and initiate inflammatory responses. This process further exacerbates the disruption of alveolus-capillary barrier integrity, leading to lung injury.

This article is protected by copyright. All rights reserved.

Accepted Article

Reference

[1] C. Wang, P. W. Horby, F. G. Hayden, G. F. Gao, *Lancet* **2020**, *395*, 470.

[2] G. Wong, Y.-H. Bi, Q.-H. Wang, X.-W. Chen, Z.-G. Zhang, Y.-G. Yao, *Zoological Research* **2020**, *41*, 213.

[3] F. Wu, S. Zhao, B. Yu, Y. M. Chen, W. Wang, Z. G. Song, Y. Hu, Z. W. Tao, J. H. Tian, Y. Y. Pei, M. L. Yuan, Y. L. Zhang, F. H. Dai, Y. Liu, Q. M. Wang, J. J. Zheng, L. Xu, E. C. Holmes, Y. Z. Zhang, *Nature* **2020**, *579*, 265.

[4] W. B. Yu, G. D. Tang, L. Zhang, R. T. Corlett, *Zool Res* **2020**, *41*, 247.

[5] C. Huang, Y. Wang, X. Li, L. Ren, J. Zhao, Y. Hu, L. Zhang, G. Fan, J. Xu, X. Gu, Z. Cheng, T. Yu, J. Xia, Y. Wei, W. Wu, X. Xie, W. Yin, H. Li, M. Liu, Y. Xiao, H. Gao, L. Guo, J. Xie, G. Wang, R. Jiang, Z. Gao, Q. Jin, J. Wang, B. Cao, *Lancet* **2020**, *395*, 497.

[6] N. Zhu, D. Zhang, W. Wang, X. Li, B. Yang, J. Song, X. Zhao, B. Huang, W. Shi, R. Lu, P. Niu, F. Zhan, X. Ma, D. Wang, W. Xu, G. Wu, G. F. Gao, W. Tan, I. China Novel Coronavirus, T. Research, *N Engl J Med* **2020**, *382*, 727.

[7] J. F. Chan, S. Yuan, K. H. Kok, K. K. To, H. Chu, J. Yang, F. Xing, J. Liu, C. C. Yip, R. W. Poon, H. W. Tsoi, S. K. Lo, K. H. Chan, V. K. Poon, W. M. Chan, J. D. Ip, J. P. Cai, V. C. Cheng, H. Chen, C. K. Hui, K. Y. Yuen, *Lancet* **2020**, *395*, 514.

[8] R. Wolfel, V. M. Corman, W. Guggemos, M. Seilmaier, S. Zange, M. A. Muller, D. Niemeyer, T. C. Jones, P. Vollmar, C. Rothe, M. Hoelscher, T. Bleicker, S. Brunink, J. Schneider, R. Ehmann, K. Zwirglmaier, C. Drosten, C. Wendtner, *Nature* **2020**, *581*, 465.

[9] Z. Xu, L. Shi, Y. Wang, J. Zhang, L. Huang, C. Zhang, S. Liu, P. Zhao, H. Liu, L. Zhu, Y. Tai, C. Bai, T. Gao, J. Song, P. Xia, J. Dong, J. Zhao, F. S. Wang, *Lancet Respir Med* **2020**, *8*, 420.

[10] L. Bao, W. Deng, B. Huang, H. Gao, J. Liu, L. Ren, Q. Wei, P. Yu, Y. Xu, F. Qi, Y. Qu, F. Li, Q. Lv, W. Wang, J. Xue, S. Gong, M. Liu, G. Wang, S. Wang, Z. Song, L. Zhao, P. Liu, L. Zhao, F. Ye, H. Wang, W.

This article is protected by copyright. All rights reserved.

Accepted Article

Zhou, N. Zhu, W. Zhen, H. Yu, X. Zhang, L. Guo, L. Chen, C. Wang, Y. Wang, X. Wang, Y. Xiao, Q. Sun, H. Liu, F. Zhu, C. Ma, L. Yan, M. Yang, J. Han, W. Xu, W. Tan, X. Peng, Q. Jin, G. Wu, C. Qin, *Nature* **2020**.

[11] D. Blanco-Melo, B. E. Nilsson-Payant, W. C. Liu, S. Uhl, D. Hoagland, R. Moller, T. X. Jordan, K. Oishi, M. Panis, D. Sachs, T. T. Wang, R. E. Schwartz, J. K. Lim, R. A. Albrecht, B. R. tenOever, *Cell* **2020**, *181*, 1036.

[12] M. Hoffmann, H. Kleine-Weber, S. Schroeder, N. Kruger, T. Herrler, S. Erichsen, T. S. Schiergens, G. Herrler, N. H. Wu, A. Nitsche, M. A. Muller, C. Drosten, S. Pohlmann, *Cell* **2020**, *181*, 271.

[13] Y. Han, L. Yang, X. Duan, F. Duan, B. E. Nilsson-Payant, T. M. Yaron, P. Wang, X. Tang, T. Zhang, Z. Zhao, Y. Bram, D. Redmond, S. Houghton, D. Nguyen, D. Xu, X. Wang, S. Uhl, Y. Huang, J. L. Johnson, J. Xiang, H. Wang, F. C. Pan, L. C. Cantley, B. R. tenOever, D. D. Ho, T. Evans, R. E. Schwartz, H. J. Chen, S. Chen, *bioRxiv* **2020**.

[14] T. Suzuki, Y. Itoh, Y. Sakai, A. Saito, D. Okuzaki, D. Motooka, S. Minami, T. Kobayashi, T. Yamamoto, T. Okamoto, K. Takayama, **2020**.

[15] R. D. Jiang, M. Q. Liu, Y. Chen, C. Shan, Y. W. Zhou, X. R. Shen, Q. Li, L. Zhang, Y. Zhu, H. R. Si, Q. Wang, J. Min, X. Wang, W. Zhang, B. Li, H. J. Zhang, R. S. Baric, P. Zhou, X. L. Yang, Z. L. Shi, *Cell* **2020**, *182*, 50.

[16] W. Deng, L. L. Bao, J. N. Liu, C. Xiao, J. Y. Liu , J. Xue, Q. Lv, F. F. Qi, H. Gao, P. Yu, Y. F. Xu, Y. J. Qu, F. D. Li, Z. G. Xiang, H. S. Yu, S. R. Gong, M. Y. Liu, G. P. Wang, S. Y. Wang, Z. Q. Song, Y. Liu, W. J. Zhao, Y. L. Han, L. N. Zhao, X. Liu, Q. Wei, C. Qin, *Science* **2020**, *369*, 818.

[17] D. Huh, B. D. Matthews, A. Mammoto, M. Montoya-Zavala, H. Y. Hsin, D. E. Ingber, *Science* **2010**, *328*, 1662.

[18] H. J. Kim, D. Huh, G. Hamilton, D. E. Ingber, *Lab Chip* **2012**, *12*, 2165.

[19] S. N. Bhatia, D. E. Ingber, *Nat Biotechnol* **2014**, *32*, 760.

[20] A. Agarwal, J. A. Goss, A. Cho, M. L. McCain, K. K. Parker, *Lab Chip* **2013**, *13*, 3599.

This article is protected by copyright. All rights reserved.

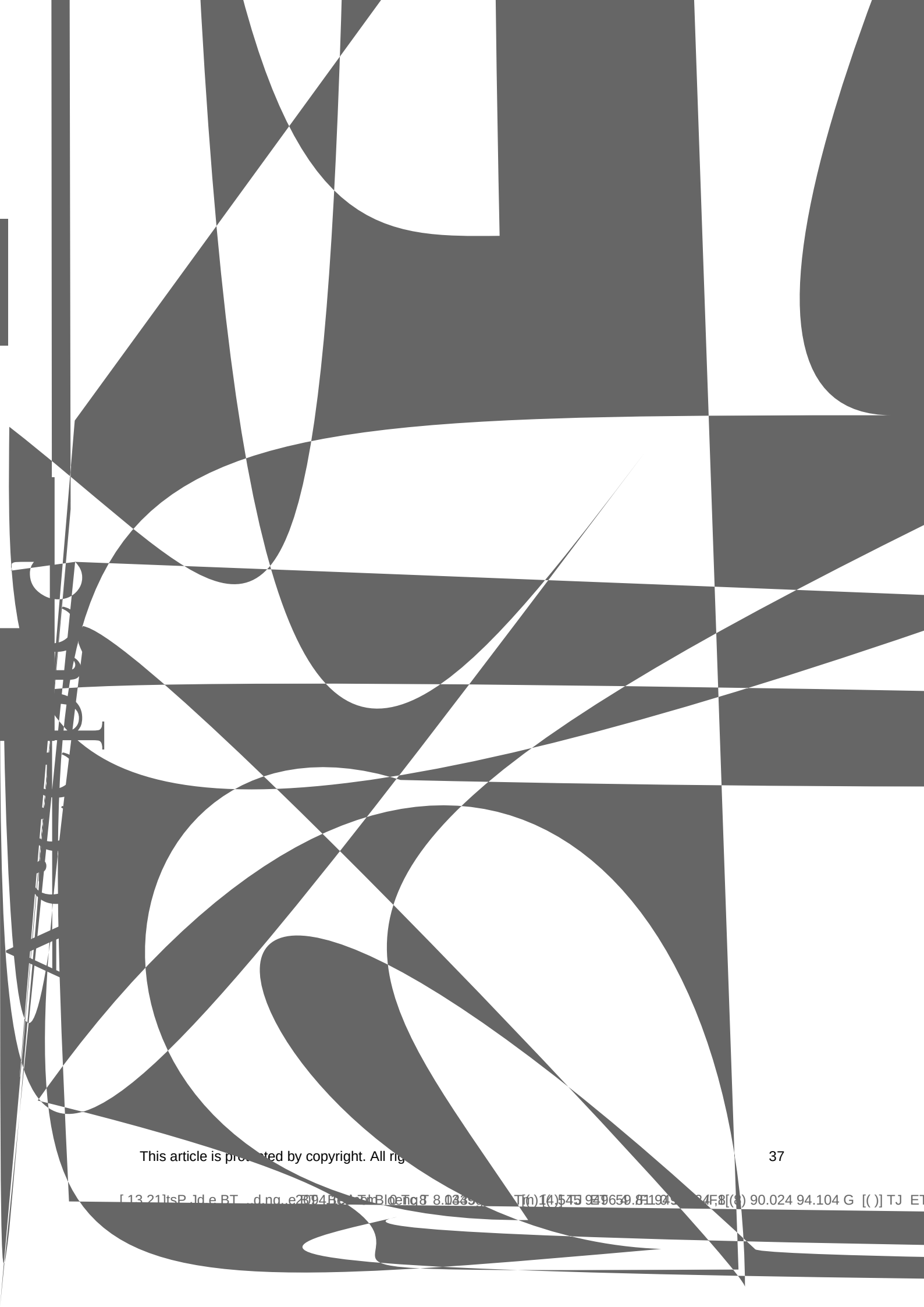

This article is protected by copyright. All rights reserved.

[13.21 ltsP Jd e BT ..d ng..e 2 94 Ft 5h Bl e Tm 8 0 Tc 8 0 Tw 14 545 94 650 8 1 94 4F 8 [( ) 90.024 94.104 G [( )] TJ ET

Accepted Article

[34] J. Harcourt, A. Tamin, X. Lu, S. Kamili, S. K. Sakthivel, J. Murray, K. Queen, Y. Tao, C. R. Paden, J. Zhang, Y. Li, A. Uehara, H. Wang, C. Goldsmith, H. A. Bullock, L. Wang, B. Whitaker, B. Lynch, R. Gautam, C. Schindewolf, K. G. Lokugamage, D. Scharton, J. A. Plante, D. Mirchandani, S. G. Widen, K. Narayanan, S. Makino, T. G. Ksiazek, K. S. Plante, S. C. Weaver, S. Lindstrom, S. Tong, V. D. Menachery, N. J. Thornburg, *Emerg Infect Dis* **2020**, *26*, 1266.

[35] X. Qin, W. Fu, Y. Zhao, Q. Meng, C. You, Q. Yu, *Biomed Res Int* **2013**, *2013*, 240659.

[36] M. Zhang, Y. Xie, R. Yan, H. Shan, J. Tang, Y. Cai, J. Yin, M. Chen, J. Zhang, X. Yang, Q. Zhang, Y. Li, *Life Sci* **2016**, *164*, 1.

[37] H. Zhang, P. Zhou, Y. Wei, H. Yue, Y. Wang, M. Hu, S. Zhang, T. Cao, C. Yang, M. Li, G. Guo, X. Chen, Y. Chen, M. Lei, H. Liu, J. Zhao, P. Peng, C. Y. Wang, R. Du, *Ann Intern Med* **2020**, *172*, 629.

[38] J. M. Nicholls, L. L. Poon, K. C. Lee, W. F. Ng, S. T. Lai, C. Y. Leung, C. M. Chu, P. K. Hui, K. L. Mak, W. Lim, K. W. Yan, K. H. Chan, N. C. Tsang, Y. Guan, K. Y. Yuen, J. S. Peiris, *Lancet* **2003**, *361*, 1773.

[39] S. Tian, W. Hu, L. Niu, H. Liu, H. Xu, S. Y. Xiao, *J Thorac Oncol* **2020**, *15*, 700.

[40] M. Wang, R. Cao, L. Zhang, X. Yang, J. Liu, M. Xu, Z. Shi, Z. Hu, W. Zhong, G. Xiao, *Cell Res* **2020**, *30*, 269.

[41] B. N. Williamson, F. Feldmann, B. Schwarz, K. Meade-White, D. P. Porter, J. Schulz, N. van Doremalen, I. Leighton, C. Kwe Yinda, L. Perez-Perez, A. Okumura, J. Lovaglio, P. W. Hanley, G. Saturday, C. M. Bosio, S. Anzick, K. Barbian, T. Cihlar, C. Martens, D. P. Scott, V. J. Munster, E. de Wit, *bioRxiv* **2020**.

[42] W. Yin, C. Mao, X. Luan, D. D. Shen, Q. Shen, H. Su, X. Wang, F. Zhou, W. Zhao, M. Gao, S. Chang, Y. C. Xie, G. Tian, H. W. Jiang, S. C. Tao, J. Shen, Y. Jiang, H. Jiang, Y. Xu, S. Zhang, Y. Zhang, H. E. Xu, *Science* **2020**, *368*, 1499.

[43] R. J. Mason, *Am J Physiol Lung Cell Mol Physiol* **2020**, *319*, L115.

[44] J. S. Lee, S. Park, H. W. Jeong, J. Y. Ahn, S. J. Choi, H. Lee, B. Choi, S. K. Nam, M. Sa, J. S. Kwon, S. J. Jeong, H. K. Lee, S. H. Park, S. H. Park, J. Y. Choi, S. H. Kim, I. Jung, E. C. Shin, *Sci Immunol* **2020**, *5*.

This article is protected by copyright. All rights reserved.

Accept

This article is protected by copyright. All rights reserved.

Accepted Article

Coronavirus disease 2019 (COVID-19) is a global pandemic caused by severe acute respiratory syndrome coronavirus 2 (SARS-CoV-2). Here, we first build a biomimetic human alveolar infection model using organ chip that allows to recapitulate the lung injury and immune responses induced by SARS-

This article is protected by copyright. All rights reserved.